Structural and magnetic properties of frustrated GaxMn(3-x)O4(1.2 ≤ x ≤ 1.6) spinels

Boubker Mehdaoui, R. Moubah, B. Orayech, M. Bahout, O. Peña, M. Jáuregui, D. Saurel, A. El Bouari

Structural and magnetic properties of frustrated $Ga_xMn_{(3-x)}O(1.2 \leq x \leq 1.6)$ spinels

B. Mehdaoui[a,b,*], R. Moubah[c], B. Orayech[d], M. Bahout[b], O. Peña[b], M. Jáuregui[d], D. Saurel[d], A. El Bouari[a]

[a]*LPCMA, Faculté des Sciences Ben M'Sik, Université Hassan II de Casablanca, B.P 7955, Casablanca, Morocco*
[b]*Institut des Sciences Chimiques de Rennes, UMR 6226, Université de Rennes 1, 35042 Rennes, France*
[c] *LPMMAT, Faculté des Sciences Ain Chock, Université Hassan II de Casablanca, B.P. 5366 Casablanca, Morocco*
[d]*CIC Energigune, Albert Einstein 48, 01510 Miñano, Alava, Spain*
[*]*Corresponding author: boubker.mehdaoui@gmail.com*

ABSTRACT

We report a systematic study of the structural and magnetic properties of frustrated compounds of $Ga_xMn_{(3-x)}O_4$ ($1.2 \leq x \leq 1.6$) prepared by solid-state reaction. Using Rietveld refinement of X-ray diffraction patterns and O'Neill-Navrotsky model, we demonstrate that the system $Ga_xMn_{(3-x)}O_4$ ($1.2 \leq x \leq 1.6$) is an inverse spinel with low inversion parameter, in which Ga^{3+} replaces Mn^{3+} cations located in B-sites. The inverse magnetic susceptibility, the shape of ZFC/FC magnetization curves at low temperatures, the existence of hysteresis in all compounds, the frustration parameter and the spontaneous magnetization analysis show that the compounds with x = 1.2-1.4 exhibit a non-collinear ferrimagnetic order and the compounds with x = 1.5-1.6 exhibit a frustrated non-collinear ferrimagnetic order. Spin wave stiffness parameters were determined for each composition using the fitting results of spontaneous magnetization curves. It is demonstrated that for the compounds x = 1.2 - 1.4 with a non-frustrated ferrimagnetic order, the change of spontaneous magnetization Ms(T) obeys to Bloch's law ($T^{3/2}$). For x = 1.5 - 1.6, the compounds exhibit a frustrated ferrimagnetic order, and the Ms(T) shows a deviation from Bloch's law.

Keywords: Spinel, Cation distribution, Ferrimagnetism, Magnetic frustration, Spin wave Stiffness parameter.

1. Introduction

Magnetic spinels with general formula AB_2O_4 are a large class of oxides with remarkable magnetic properties which make them interesting for both the fundamental and technological

levels. They are promising in a wide range of applications such as multiferroic devices[1], spintronics[2], cathode materials with high energy densities[3], microwaves[4], sensors for *ac* and *dc* magnetic fields[5], magnetic hyperthermia[6], and magnetic refrigeration[7]. The diversity of their magnetic properties is associated with the complexity of their magnetic structure which leads to peculiar effects, such as magnetic frustration or multiferroicity. In spinel structure AB_2O_4, the *A* ions occupy tetrahedral sites and B ions occupy octahedral sites. The B sites form a pyrochlore network of tetrahedrons linked by their vertices; the antiferromagnetic interactions between the first neighbors B lead to strong magnetic frustration[8]. The diamond-like network A has an antiferromagnetic collinear order with long-range magnetic frustration; this frustration is due to a competition between the interactions of the first, second and third neighbors[9,10]. The frustration could also be originated from the chemical disorder or competition of J_{AA}, J_{AB} and J_{BB} interactions, as in spin glasses[11,12]. As a consequence, the substitution in two sublattices A and B, occupied by magnetic ions, by different magnetic or diamagnetic ions, lifts a part of the degeneration and leads to magnetic states which can break the inversion symmetry and allow the appearance of fascinating physical effects[13]. In this perspective, the Mn_3O_4 is an interesting compound to investigate the influence of ion substitution on its magnetic properties. Mn_3O_4 crystallizes in the $I4_1/amd$ space group, it is a normal spinel with Mn^{2+} divalent ions in tetrahedral sites (A) and Mn^{3+} trivalent ions in octahedral sites (B). It shows a non-collinear magnetic order below Tc ≈ 42K[14], while below 33K the magnetic structure is non-collinear of the Yafet-Kittel type. The moments of Mn^{2+} ions (A) are directed along the [010] axis and the Mn^{3+}ones (B), located in the plane (100), are divided into two sublattices, each forming an angle of 69° with the [010] axis so that the resulting B moment is antiparallel to that of the A site. Between 33 and 39K the B magnetic moments form a spiral with a propagation of the magnetic moment along the [010] axis, and between 39 and 42 K, the structure is collinear with Néel type[15]. In addition, using neutron diffraction, it was shown a complex magnetic structure with a diffuse scattering component characteristic of a short order distance which persists at room temperature due to the geometric frustration imposed by the pyrochlore network B[16]. Therefore, it is interesting to study the magnetic behavior of the $Ga_xMn_{3-x}O_4$ system ($1.2 \leq x \leq 1.6$), where the substitution takes place in the pyrochlore network, the sublattice A being occupied by a magnetic ion Mn^{2+}. The synthesis and structural properties of $Ga_xMn_{3-x}O_4$ were recently studied[17]. However, no study concerning the magnetic properties was reported on the $Ga_xMn_{3-x}O_4$ system. It is known that in spinels, the cation distribution in octahedral and tetrahedral sites strongly influences the structural and magnetic properties; the cation distribution in these two

sites are subjected to many factors, such as the preparation method, temperature and eventual impurities[18]. So, it is important to determine the cation distribution for each system. Several studies were made to characterize the cation distribution in spinels and related their thermodynamic properties to structural information [19, 20, 21, 22, 23]. O'Neill and Navrotsky [24, 25] developed a thermodynamic model, widely used to calculate the cation distribution from thermodynamic constants [26, 27, 28, 29, 30, 31]. In this work we present the synthesis of the solid solution $Ga_xMn_{(3-x)}O_4$ (x = 1.2-1.6), we discuss the structural properties according to the structural parameters (cell parameters and cationic distribution), we use different models for Rietveld refinement, and O'Neill and Navrotsky's model to calculate the cationic distribution in different sites from the thermodynamic constants. We also present a study of the magnetic properties using magnetization measurements; the detailed relationship between the structural and magnetic properties was also investigated.

2. Experimental

Polycrystalline $Ga_xMn_{(3-x)}O_4$ ($0 \leq x \leq 2$) compounds were synthesized using solid-state reaction method. Stoichiometric amounts of Mn_2O_3 and Ga_2O_3 (purity 99%) were mixed, grounded and annealed at 1000°C during 48h. The obtained powder was then pressed into 13 mm-diameter pellets at 377 MPa, annealed in air at 1100°C for 48h and heated at 1350°C for 24h. The cooling rate was set at 1°C/min. X-ray diffraction (XRD) measurements were performed at room temperature for all samples using Panalytical X'Pert Pro diffractometer. The recording was carried out with a wavelength λ = 1.5405Å, in the angular range $16° < 2\theta < 130°$ with a counting step of 0.0083°. The data were analysed using Rietveld method as implemented in the Fullprof program [32]. The changes of magnetization as function of temperature under a fixed value of applied magnetic field were performed in two temperature ranges using Quantum Design MPMS-XL5 SQUID magnetometer, from 5 - 300K under an applied magnetic field of 0.1T and through zero-field cooling (ZFC) and field cooling (FC) procedures on the temperature range 2 – 50K at an applied magnetic field of 0.005 T. Magnetization measurements as function of applied magnetic field were carried out in two magnetic field ranges, i) hysteresis loops were recorded at 2K from -5T up to +5T; and ii) first magnetization measurements from 0T up to 9T at different temperatures using Physical Property Measurement System (PPMS) from Quantum Design. The spontaneous magnetizations Ms(T) were determined by extrapolation to H = 0T of the linear variation of M (H) near saturation.

3. Results and discussion

3.1. Structural properties

According to the XRD patterns of the $Ga_xMn_{3-x}O_4$ samples ($0 \leq x \leq 2$) obtained after annealing at 1350°C for 24h, four regions can be deduced. For $0 \leq x \leq 0.2$, the patterns show characteristic peaks of a single tetragonal spinel phase typical of Mn_3O_4. When $0.3 \leq x \leq 1.1$, the patterns indicate the coexistence of two phases: cubic and tetragonal. For $1.2 \leq x \leq 1.6$, only one phase is observed which corresponds to cubic spinel with *Fd-3m* space group. For $x \geq 1.7$, the XRD data suggest the presence of a cubic spinel phase and Ga_2O_3 as a secondary phase (see Fig. SI-1).

In the following, we only investigate the single-phase $Ga_xMn_{3-x}O_4$ ($1.2 \leq x \leq 1.6$) system. The analysis of XRD patterns for $1.2 \leq x \leq 1.6$ shows a solid solution domain, characterized by a single phase indexed in cubic spinel structure. As can be seen from Figure 1(a), all the phases show the same peaks distribution. A shift of the Bragg peak towards higher Bragg angles with the increase of Ga content, which means that the unit cell gets smaller, and the variation of the peak intensities with increasing x(Ga^{3+}), as evident from Figure (SI-2), is a manifestation of the substitution effect in the system.

The structural refinements were carried out by Rietveld method using the FullProf program. The cubic $MgAl_2O_4$ with *Fd-3m* space group was the starting structural model used in our refinements[33]. The oxygen ions are located in the 32e position; the tetrahedral sites A are in 8a positions, while the octahedral sites B are in the 16d positions. The refined parameters were the lattice parameter (*a*), the oxygen atomic coordinates (*u*), the occupancy of the tetrahedral and octahedral sites and the atomic displacement parameters of all atoms. The peak shapes were described using a pseudo-Voigt function. The first step of refinement was to determine the correct cell parameters using a cubic cell. For structural refinement, several models were tested. The quality of the refinements was judged based on the reliability factors (R_P, R_{wp}, R_{Bragg}, R_F-factor, and Chi^2).

The $Ga_xMn_{3-x}O_4$ ($1.2 \leq x \leq 1.6$) system consists of two different types of atoms that are distributed over the tetrahedral (A) and the octahedral (B) sites. The atomic scattering factors of Ga and Mn for X-rays are shown in Figure (SI-3). The significant difference in atomic scattering is favorable for the precise determination of the atomic occupancies. The four test models for the $Ga_{1.2}Mn_{1.8}O_4$ composition, taken as an example, are the following: a1 Model with $(Ga)_A[Ga_{0.2}Mn_{1.8}]_BO_4$, a2 Model with $(Mn_{0.5}Ga_{0.5})_A[Ga_{0.7}Mn_{1.3}]_BO_4$, a3 Model with $(Mn)_A[Ga_{1.2}Mn_{0.8}]_BO_4$ and a4 Model with $(Mn_{0.8}Ga_{0.2})_A[GaMn]_BO_4$. The results of Rietveld

refinements of the four models are shown in figure (SI-4) with their corresponding reliability factors. The results show that a3 and a4 models give the best reliability factors with R_p= 10.7% and 10.2% for models a3 and a4, respectively. The a3 model is a normal spinel $(Mn)_A[Ga_{1.2}Mn_{0.8}]_BO_4$. Based on this model, the Mn and Ga located at the octahedral site have an oxidation state of +3 while the Mn located at the tetrahedral site has a +2 oxidation state. The cation distribution for a3 model is then given by $(Mn^{2+})_A[Ga^{3+}{}_{1.2}Mn^{3+}{}_{0.8}]_BO_4$. Model a4 is an inverse spinel with low inversion parameter; 0.2 Ga^{3+} occupies the tetrahedral site and an equivalent amount of Mn^{2+} occupies the octahedral site. The cation distribution for the a4 model is in agreement with that obtained recently by Venediktova *et al.*[17].

The a3 and a4 models have similar reliability factors. In order to confirm the a4 model, we calculated the cation distribution in A and B sites according to the O'Neill and Navrotsky's model[24, 25]. It is known that the cation distribution in spinels is explained by the cation site preference. Based on literature data[31], the Mn^{3+} cations strongly prefer the octahedral sites, whereas Mn^{2+} et Ga^{3+} are randomly distributed over both tetrahedral and octahedral sites. The cation distribution in that case is given by $(Mn^{2+}{}_{1-y}Ga^{3+}{}_y)_A[Mn^{2+}{}_yGa^{3+}{}_{x-y}Mn^{+3}{}_{2-x}]_BO_4$, where (x) is the mole number of Ga introduced into the system and (y) represents the inversion parameter. The O'Neill-Navrotsky model consists in minimizing the free energy. The disordering enthalpy has a quadratic form with the inversion parameter and the disordering entropy is related to the configurational entropy[24,25]. The configuration entropy ΔS_C of the system is given by:

$$\Delta S_c = -R\left[(1-y)\ln(1-y) + y\ln y + y\ln\frac{y}{2} + (2x-y)\ln\left(\frac{x-y}{2}\right) + (2-x)\ln\left(1-\frac{x}{2}\right)\right] \quad (1)$$

A change in the cation distribution is accompanied by a change in the free energy of disorder ΔG_{cd} which is given by:

$$\Delta G_{cd}(y) = y\alpha_{Mn^{2+}-Ga^{3+}} + \beta y^2 - yT\sigma_{Mn^{2+}-Ga^{3+}} - T\Delta S_C \quad (2)$$

α and β are the interchange enthalpy parameters. It was found that for 2–3 spinels, β takes values between -15 and -25 kJ mol^{-1} and an average value of β = -20 kJ mol^{-1} can be used[27]. The parameters $\alpha_{Mn2+-Ga3+}$ and $\sigma_{Mn2+-Ga3+}$ are calculated from the values given in reference [25] for Mn^{2+} and Ga^{3+} cations; the values used in the calculation are $\alpha_{Mn2+-Ga3+}$ = 49kJ mol^{-1} and $\sigma_{Mn2+-Ga3+}$ = 0 kJmol^{-1}. At the equilibrium of the cation arrangement, the free energy will be minimum with respect to any change in the inversion parameter y, that is $\frac{\partial(\Delta G_{cd}(y)}{\partial y} = 0$, hence:

$$-RTln(\frac{y^2}{(1-y)(x-y)}) = \alpha_{Mn^{2+}-Ga^{3+}} + 2\beta y - T\sigma_{Mn^{2+}-Ga^{3+}} \quad (3)$$

Solving equation (3) allows us to calculate the inversion parameter y for each value of x at T = 1350 ° C (the synthesis temperature). Results are shown in Table 1. We find that the inversion parameter y increases slightly as a function of x (Ga^{3+}), varying between 0.16 and 0.20 for x = 1.2-1.6.

This result shows that our solid solution is an inverse spinel with a low inversion parameter, in agreement with the a4 model. Recent results on the same system showed an inversion parameter of approximately 0.20[17].

Once the a4 model was confirmed, a Rietveld refinement was performed on the $Ga_xMn_{3-x}O_4$ system with x = 1.2-1.6. Figure 1 (b) shows, as an example, the refined pattern for x = 1.2 with good agreement between the observed and calculated profiles. Table 1 displays details of the crystal structures, cell parameters, oxygen atomic coordinates, cation distribution and reliability factors for all compounds.

The obtained cell parameters are plotted versus Ga content in Figure 1 (c). These results fit perfectly well with the observed peak shift (Fig. SI-2) and confirm that the lattice parameter *a* decreases linearly with increasing Ga^{3+} content. Figure 1 (d) shows the occupancy variation of the different cations located at the tetrahedral and octahedral sites. The occupation of Mn^{3+} decreases with the increase of x(Ga^{3+}) in the octahedral site due to its progressive substitution by Ga^{3+}which increases in the same site. The octahedral site is also occupied by a small amount (y) of Mn^{2+}, while the tetrahedral site remains occupied by a fraction (1-y) of Mn^{2+} and (y) of Ga^{3+} cations. The inversion parameter (y) shows a small variation depending on the substitution, it increases from y = 0.20 to y = 0.24 for the compounds x = 1.2-1.4, and then it decreases to reach y = 0.16 for the compound x = 1.6. As said above, the cationic distribution in the octahedral and tetrahedral sites is given by $(Mn^{2+}_{(1-y)}Ga^{3+}_{y})_A[Mn^{2+}_{y}Ga^{3+}_{(x-y)}Mn^{3+}_{(2-x)}]_BO_4$. This result is consistent with that calculated using O'Neill's model which shows an inversion parameter y = 0.16-0.20.

Therefore, the decrease of lattice parameter can be attributed to the slightly smaller Ga^{3+} radius at the octahedral site compared to Mn^{3+}. In addition, in cubic spinel structures, the relationship between the lattice parameter and the distances d_{A-O} and d_{B-O} is given by the following equation[34]: $a = 2.09 + \sqrt{5.81d_B^2 - 1.41d_A^2}$ (4).

The theoretical tetrahedral and octahedral cation-anion distances d_{A-O} and d_{B-O} were calculated using Shannon ionic radii[35]: $d_A(Ga^{3+}-O)$ = 1.85Å, $d_B(Ga^{3+}-O)$ =2.00 Å ; $d_A(Mn^{2+}-O)$=2.04 Å, $d_B(Mn^{2+}-O)$=2.22 Å, $d_B(Mn^{3+}-O)$ = 2.045Å. Since more than one type atom occupies the same site, the mean distances for each site were calculated, on one hand, using Shannon ionic radii and the chemical occupancy determined from the Rietveld refinements, and on the other hand the cation distribution obtained from O'Neill's model. The calculated lattice parameters are compared in Table 1 with those obtained from the experimental data refinements. The good agreement between the lattice parameters obtained experimentally and those calculated, confirms that the substitution proceeds in the octahedral sites according to the formula $(Mn^{2+}_{(1-y)}Ga^{3+}_{y})_A[Mn^{2+}_{y}Ga^{3+}_{x-y}Mn^{3+}_{(2-x)}]_BO_4$.

3.2.Magnetic Properties

3.2.1. Paramagnetic regime

Figure 2(a) displays the change of the inverse magnetic susceptibility as a function of temperature recorded under a magnetic field of 0.1T of $Ga_xMn_{(3-x)}O_4$ powders ($1.2 \leq x \leq 1.6$). Above the magnetic ordering temperature T_C, the shape of curves is not linear, but follows a hyperbolic form typical of a ferrimagnetic system with two sublattices in antiferromagnetic interaction. These curves can be analyzed using the following equation[36]:

$$\frac{1}{\chi} = \frac{1}{\chi_0} + \frac{T}{C} - \frac{\sigma}{T-\theta} \quad (5)$$

If T >>θ, the third term becomes negligible and the hyperbolic form reduces to a linear form at high temperature; therefore the Curie-Weiss linear law can be applied [Fig.2 (b)]. Table 2 lists the fitting parameters obtained using Curie-Weiss linear equation in the temperature range from 150 to 300K. The theoretical magnetic moments were calculated using the following formula:

$$\mu_{theo} = \sqrt{\mu(Mn^{2+})^2 + (2-x)\mu(Mn^{3+})^2} \quad (6)$$

Here *x* is the Ga^{3+}content with values given by the XRD refinement. The theoretical moments of $Mn^{2+}$and Mn^{3+}can be expressed as $\mu = g\sqrt{S(S+1)}$, where g is the Landé factor (g = 2), and $S(Mn^{2+})$ = 5/2 and $S(Mn^{3+})$ = 2. In the case of x = 1.2, 1.5 and 1.6, the deduced theoretical moments μ_{theo} are in good agreement with the experimental effective magnetic moments μ_{eff}, with a difference $\Delta\mu = |\mu_{eff} - \mu_{theo}| < 1.7\%$ (see Table 2). For the compound with x = 1.3, a small difference $\Delta\mu$ = 3% was observed. The compound x = 1.4 has a

difference of $\Delta\mu$ = 4.8%. In general, the effective moments show a nice agreement with the theoretical moments with a difference $\Delta\mu$ <5 %. This small difference could be attributed to the presence of impurities non-detectable by XRD such as Mn_3O_4.

By increasing x(Ga^{3+}), the effective magnetic moment decreases due to the substitution of Mn^{3+} by non-magnetic Ga^{3+}ions. The large and negative Curie-Weiss temperature θ indicates the existence of strong antiferromagnetic coupling between two sublattices. The absolute value of θ decreases with increasing Ga^{3+} content, highlighting that the insertion of non-magnetic ions into the B sites reduces the interactions between A and B networks. The magnetic ordering temperature T_C was determined from the minimum of the magnetization derivative as a function of temperature, as it will be discussed later; T_C shows a gradual decrease with increasing x. For x = 1.2 and 1.3, the magnetic frustration parameter $f = \theta/T_C$ is less than 10, indicating that the magnetic order in both compounds is a long-range order[37]. With further increasing x (Ga^{3+}), the f parameter increases, suggesting the appearance of a short-range order due to disorder of magnetic interactions introduced by the non-magnetic Ga^{3+} ions.

3.2.2. Ordered regime

To have further information on the magnetic interactions in the ferrimagnetic state, we have performed ZFC/FC measurements at 5mT and hysteresis loops M(H) at 2K, for the five compositions. Figure 3 (a) displays the ZFC/FC curves of $Ga_xMn_{3-x}O_4$ ($1.2 \leq x \leq 1.6$). We note the existence of irreversibility T_{irrev} at the approach of the maximum value of ZFC magnetization. Below T_{irrev}, the ZFC magnetization decreases rapidly, a behavior typical of antiferromagnetic interactions. For x = 1.2-1.3, the ZFC magnetization becomes negative below a certain compensation temperature, confirming the existence of antiferromagnetic interactions between two sublattices. This behavior has already been observed in similar compounds based on Ni, Co and Mn, and shows a global ferrimagnetic behavior at low temperature[38, 39, 40]. The FC curves superpose the ZFC curves in the temperature range from 300 K to T_{irrev}. Below T_{irrev}, the FC magnetization increases to reach a maximum followed by a saturation at lower temperatures. This behavior is more pronounced for compositions x = 1.2, 1.3 and 1.4. This is characteristic of a P-type ferrimagnetic structure[41].The shape of the FC magnetization curve can be explained by a competition between the J_{AA}, J_{BB} and J_{AB} interactions. For x = 1.5 and 1.6, the shape of magnetization curves ZFC/FC indicates the existence of magnetic frustration in agreement with the frustration parameter (see Table 2). The transition temperature T_C decreases with magnetic dilution [Inset, Fig. 3 (a)], highlighting

an evolution towards a complex magnetic structure due to a magnetic frustration which becomes more important with dilution.

Figure 3 (b) displays the hysteresis loops as a function of the applied magnetic field at 2K for $Ga_xMn_{3-x}O_4$ ($1.2 \leq x \leq 1.6$) compounds. The change of the coercive field Hc as a function of $x(Ga^{3+})$ is displayed in the inset Fig. 3(b). The magnetization curves show a hysteresis typical of a ferrimagnetic system with an unsaturated character up to 5T, for all compounds. With increasing Ga^{3+} content, the hysteresis cycles become increasingly closer, the coercive field (Hc) and the magnetization decrease with increasing $x(Ga^{3+})$, indicating an evolution towards a complex magnetic structure.

To see the possibility of reaching saturation under a magnetic field, we have performed first magnetization curve measurements as a function of magnetic field up to 9T at different temperatures (Fig.4). For $T < T_C$, the magnetization rapidly increases for low magnetic fields, followed by a linear increase as a function of the applied magnetic field without saturation, which indicates that the magnetic structure is canted. The spontaneous magnetizations Ms (T) were deduced by extrapolating to H = 0T the linear part of the magnetization curves. The values of the spontaneous magnetization Ms (2K) determined at 2 K are listed in Table 3. The results show that Ms(2K) decreases with increasing $x(Ga^{3+})$. Quantitative information on the cation distribution in $Ga_xMn_{(3-x)}O_4$, obtained by refinement of the XRD data using Rietveld methods, is very helpful in the interpretation of the observed magnetization degradation. In the system $Ga_xMn_{(3-x)}O_4$, the Mn^{2+}(S = 5/2) cations occupy both sites A and B, and the Mn^{3+}(S = 2) cations occupy only the B sites. Under the assumption of collinear spin arrangement, the values of the spontaneous magnetization Ms can be calculated by the Néel model, expressed by $Ms = M_A(Mn^{+2}) + M_B(Mn^{+2}) - M_B(Mn^{+3})$, where M_A and M_B are the effective magnetic moments of A and B sublattices, respectively. The values of Ms obtained using the collinear model are presented in Table 3. The Ms values were found to be larger than the experimental values. This indicates that the compounds have a non-collinear ferrimagnetic structure, with the Mn^{3+} and Mn^{2+}magnetic moments in B sites being linear and antiferromagnetic, and those of Mn^{2+} in A sites making an angle φ with the direction of the total magnetization. The φ angle of each composition (Table 3) was calculated as a function of magnetic field from the first magnetization curves M(H) measured at 2K, using the following formula: $Ms(H) = M_A(Mn^{+2})\cos(\varphi(H)) + M_B(Mn^{+2}) - M_B(Mn^{+3})$.

Figure 5(a) displays, the corresponding φ(H) curve. It is found that the angle φ(H) decreases with increasing magnetic field according to an exponential function for all compounds:

$$\varphi(H) = \varphi_0 + \varphi_1 e^{\frac{-H}{H_0}} \qquad (7)$$

The fitting by this equation allows to determine the canting angle φ_0 at strong magnetic field (H tends to infinity), and also determines the ($\varphi_0 + \varphi_1$) canting angle at zero magnetic field (H = 0T). The term H_0 is a mean field that represents the magnetic interactions; it includes the exchange interaction between the magnetic moments and the magnetic anisotropy. The results of the fit are shown in Figure 5(a), and in Table 3 we present the obtained fit parameters φ_0, φ_1 and H_0.

The ($\varphi_{0+}\varphi_1$) values which represent the canting angle at zero magnetic field were found to increase with increasing *x(Ga^{3+})* (Figure 5 (b)) showing an evolution towards an antiferromagnetic structure in the A sites with the substitution of Mn^{3+} ions by non-magnetic Ga^{3+} ions in B sites. At zero magnetic field and at T = 2K, the compounds stabilize in a non-collinear ferrimagnetic structure, in which the magnetic moments of Mn^{3+} and Mn^{2+} ions are collinear in the B sites and those of Mn^{2+} ions in A sites form an angle ($\varphi_{0\ +}\varphi1$)with the direction of total magnetization.

Under a strong magnetic field, the magnetic structure remains non-collinear with an angle of φ_0 smaller than that observed at zero magnetic field (Fig.5 (b)).

The H_0 parameter, which represents the effects of magnetic interactions, shows a decrease between the compounds x = 1.2-1.4, due to the introduction of non-magnetic ions into the system. For compounds x = 1.5-1.6, the observed increase may be related to the effects of magnetic frustration (See Table 3).

In summary, the shape of the inverse magnetic susceptibility, the shape of the ZFC/FC magnetization curves at low temperatures, the existence of hysteresis in all compounds, the frustration parameter and the spontaneous magnetization analyses show that the compounds present a non-collinear ferrimagnetic order, and with further increasing x(Ga^{3+}), the frustration parameter f increases, suggesting the appearance of a short-range order, which coexists with a non-collinear ferrimagnetic state.

3.2.3. Determination of spin wave stiffness parameters

Using spin waves theory[42], we determine the spin wave stiffness parameter D from the temperature dependence of magnetization. For systems with two magnetic sublattices, A (tetrahedral sites) and B (octahedral sites), the dispersion relation for acoustic magnons to order k^2 can be expressed as[43,44] : $\overline{h}\omega = Dk^2$,

ω is the frequency, k is the spin wave momentum. The temperature dependence of magnetization M(T) follows Bloch's law ($T^{3/2}$) which is associated to the thermal excitation of spin waves. The M (T) curves can be expressed as [45, 46]:

$$\frac{M_S(T)}{M_S(0K)} = 1 - \frac{0.0568}{4(S_A - 2S_B)}\left(\frac{a^2 k_B}{D}\right)^{3/2} T^{3/2} = 1 - BT^{3/2} \quad (8)$$

Spin-wave stiffness parameter with the notation D is given by the following formula:

$$D = \left(\frac{0.0568}{8(M/\mu_B)}\right)^{\frac{2}{3}} \frac{a^2 k_B}{B^{\frac{2}{3}}} \quad (9)$$

Here *a* is the unit cell parameter, M is the spontaneous magnetization, k_B is the Boltzman constant and B is the Bloch constant.

In order to determine the spin wave stiffness parameters D from the temperature dependence of magnetization below T_C using the results of spin wave theory, we have plotted in Fig. 6, the change of Ms (T) as a function of temperature for the different samples. We note that Ms (T) decreases with increasing temperature due to the spin-wave excitations.

The Ms(T) curves were fitted using equation (8) (Bloch's law). The results of fits are presented in Fig.7.

We find that for samples with x = 1.2 and 1.4, the change of the spontaneous magnetization with temperature is in line with Bloch's law. However, for the samples x = 1.5 and 1.6, the experimental Ms(T) deviates from $T^{3/2}$ law. The Ms(T) change can then be modeled using Dyson approximation[47]:

$$\frac{M_S(T)}{M_S(0K)} = 1 - BT^{3/2} - CT^{5/2} \quad (10)$$

Bloch's constants B and D parameters calculated using equation (9) are listed in Table 3. These results indicate that we have two sets of compounds with two different magnetic behaviors, the samples x = 1.2-1.4 and the compounds x = 1.5-1.6. These observations are in line with the results reported by Efimova and Kufterina on the magnetic properties of dilute frustrated ferromagnetic spinels $Li_{0.5}Fe_{(2.5-x)}Ga_xO_4$ [48]. They have shown that the Ms(T) curves for the frustrated ferrimagnets do not obey Bloch $T^{3/2}$ law, which is satisfied in the absence of frustrations. If the collinear ferrimagnetic ordering is restored by applying an external magnetic field, the Ms(T) curves could be described using Dyson approximation (Eq. 10). Thus, we conclude that our samples x = 1.2-1.4 present a non frustrated ferrimagnetic order,

and that samples x = 1.5-1.6 present a frustrated ferrimagnetic order. This frustration is attributed to chemical disorder caused by the introduction of non-magnetic ions into the octahedral sites. In these compounds, frustration can also be caused by a competition between the interactions of the first, second and third neighbors as in spin glasses.

Spin wave stiffness parameters D are shown in Table 3 for four compounds. For non-frustrated compounds x = 1.2-1.4, D decreases with the introduction of a non-magnetic cation into B sites, D = 53 - 40meV $Å^2$, D calculated from Bloch equation (8). These D values are five times smaller than those obtained in the ferrimagnetic $Mg_xFe_{3-x}O_4$ compounds (296 - 202 meV $Å^2$)[49], due to the stronger J_{AB} interactions in the ferrites.

For the frustrated compounds (x = 1.5-1.6), we note that D increases as a function of x (D = 82 -135meV $Å^2$), D calculated using Dyson equation (10). The evaluated D values are close to those for ferromagnetic glasses (≈100 meV$Å^2$)[50]. In perspective, an accurate determination of the spin wave stiffness parameters D requires measurements of the magnon-dispersion relations performed by magnetic elastic neutrons scattering or Brillouin light scattering.

4. Conclusions

By analyzing the XRD data refined using Rietveld methods, we have shown that the system $Ga_xMn_{(3-x)}O_4$ ($1.2 \leq x \leq 1.6$) is an inverse spinel with low inversion parameter, in which Ga^{3+} ions replace the Mn^{3+} cations located in B-sites, in agreement with the O'Neill-Navrotsky model. The cation distribution is given by $(Mn^{2+}_{1-y}Ga^{3+}_{y})_A[Mn^{2+}_{y}Ga^{3+}_{x-y}Mn^{+3}_{2-x}]_BO_4$.

Magnetic information was extracted from the curves of the inverse magnetic susceptibility, the ZFC/FC magnetization, the first magnetization and hysteresis curves. The shape of inverse magnetic susceptibility is a hyperbolic form typical of a ferrimagnetic system. The calculated moments μ_{theo} are in agreement with the experimental effective magnetic moments μ_{eff}, and confirm the cation distribution. For x = 1.2 and 1.3, the magnetic frustration parameter $f = \theta/T_C$ is less than 10, indicating that the magnetic order in both compounds is a long-range order. With further increasing x(Ga^{3+}), the f parameter increases, suggesting the appearance of a short-range order. The shape of the ZFC/FC magnetization curves at low temperatures, the existence of hysteresis in all compounds, and the spontaneous magnetization analyses show that the compounds x = 1.2-1.4 have a non-collinear ferrimagnetic order and the compounds x = 1.5-1.6 have a frustrated non-collinear ferrimagnetic order. It has been established that for compounds with x = 1.2 and 1.4 with a non-frustrated ferrimagnetic order, the temperature dependence of the spontaneous magnetization Ms(T) obeys to Bloch's law with exponent $T^{3/2}$. For x = 1.5 and 1.6, compounds with frustrated ferrimagnetic order, a deviation from Bloch's

law was seen, the Ms(T) curves being described using Dyson approximation (exponents $T^{3/2}$ and $T^{5/2}$). Spin wave stiffness parameters were determined for each composition from the fits of Ms(T) using Bloch's law. This study will be very useful to understand the magnetic properties of $Ga_xMn_{(3-x)}O_4$ compounds.

Conflicts of interest

There are no conflicts of interest to declare.

Acknowledgements

In memory of Arlei B. Antunes (1967–2010), whose invaluable comments concerning the magnetic properties, helped to carry this work to term.

Appendix A. Supplementary data

Supplementary data related to this article can be found at XXXX

References :

[1]N. Ortega, Ashok Kumar, J. F. Scott and Ram S. Katiyar, Journal of Physics: Condensed Matter, 27 (2015) 504002.

[2]D. J. Hagen, T. S. Tripathi and M. Karppinen, Dalton Trans., 46 (2017) 4796.

[3] D. Liu, W. Zhu, J. Trottier, C. Gagnon, F. Barray, A. Guerfi, A. Mauger, H. Groult, C. M. Julien, J. B. Goodenough and K. Zaghib, RSC Adv., 4 (2014) 154.

[4] M. Pardavi-Horvath, J. Magn. Magn. Mater., 215 (2000) 171.

[5]Y. K. Fetisov, A. A. Bush, K. E. Kamentsev, A. Y. Ostashchenko, and G. Srinivasan, IEEE Sensors Journal, 6 (2006) 935.

[6]Wei Zhang, Xudong Zuo, Ying Niu, Chengwei Wu, Shuping Wang, Shui Guan and S. Ravi P. Silva, Nanoscale, 9 (2017) 13929-13937.

[7]M. Bouhbou, R. Moubah, W. Belayachi, A. Belayachi and H. Lassri, Dalton Trans., 46 (2017) 2007.

[8] A. P. Ramirez, Annu. Rev. Matter. Sci., 24 (1994) 453.

[9] N. Büttgen, J. Hemberger, V. Fritsch, A. Krimmel, M. Mücksch, H-A Krug von Nidda, P.Lunkenheimer, R. Fichtl, V. Tsurkan and A. Loidl, New J. Phys. 6 (2004) 191.

[10] V. Fritsch, J. Hemberger, N. Büttgen, E-W. Scheidt, H-A. Krug von Nidda, A. Loidl and V. Tsurkan, Phys. Rev. Lett., 92, (2004) 92 116401.

[11] E. Vincent, J. Hammann and M. Alba, Solid State Commun, 58 (1986) 57.

[12]Ram A. Pawar, Sunil M. Patange and Sagar E. Shirsath, RSC Adv., 6 (2016) 76590.

[13]Ingyu Kim, Yoon Seok Oh, Yong Liu, Sae Hwan Chun, Jun-Sik Lee, Kyung-Tae Ko, Jae-Hoon Park, Jae-Ho Chung, and Kee Hoon Kim, Appl. Phys. Lett., 94 (2009) 042505.

[14] B. Boucher, R. Buhl and M. Perrin, J. Phys. Chem. Solids, 32 (1971) 2429.

[15] G. B. Jensen and O. V. Nielsen, J. Phys. C: Solid State Phys., 7 (1974) 409.

[16] A. Kuriki, Y. Moritomo, S. Xu, K. Ohoyama, K. Kato and A. Nakamura, J. Phys. Soc. Jpn., 72 (2003) 458.

[17] O.S. Venediktova, O.A. Bulavchenko, T.N. Afonasenko, P.G. Tsyrul'nikov, Z.S. Vinokurov, Yu. A. Chesalov and S.V. Tsybulya, Journal of Alloys and Compounds, 725 (2017) 496-503.

[18] N.G. Jovic, A.S. Masadeh, A.S. Kremenovic, B.V. Antic, J.L. Blanusa, N.D. Cvjeticanin, G.F. Goya, M.V. Antisari and E.S. Bozin, J. Phys. Chem. C, 112 (2009) 20559

[19] A. Petric, K. T. Jacob, and C. B. Alcock, Journal of the American Ceramic Society, 64 (1981) 632.

[20] A. Petric and K. T. Jacob, Solid State Ionics, 6, 1982, 47-56.

[21] K. T. Jacob and G. N. K. Iyengar, J. Am. Ceram. Soc., 69 (1986) 487

[22]H.-I. Yoo and H. L.Tuller, J. Phys. Chem. Solids, 49 (7) (1988) 761-766.

[23] Bong-HoonPark and Hideaki Suito, Thermochimica Acta, 205 (1992) 289-298.

[24] H. S. C. O'Neill and A. Navrotsky, Am. Mineral., 68 (1983) 181–194.

[25] H. S. C. O'Neill and A. Navrotsky, Am. Mineral., 69 (1984) 733–753.

[26] K. Leinenweber and A. Navrotsky, Phys. Chem. Minerals 16 (1989) 497-502

[27] H. S. C. O'Neill and W. A. Dollase, Phys. Chem. Minerals, 20 (1994) 541-555.

[28] Q. Wei and B. W. Robertson, Journal of Solid State Chemistry, 176 (2003) 279–283.

[29] H. ST.C. O'Neill, M. James, W. Dollase, and S. T. Redfern, Eur. J. Mineral., 17 (2005) 581-586.

[30]K. I. Lilova, K. Shih, C.-W.Pao, J.-F. Lee and A. Navrotsky, J. Am. Ceram. Soc., 95 (2012) 423–430

[31] S. K. Sahu, B. Huang, K. Lilova, B. F. Woodfield, and A. Navrotsky, Phys. Chem. Chem. Phys., 17 (2015) 22286.

[32] J. Rodriguez-Carvajal, Physica B, 192 (1993) 55.

[33] R. J. Hill, J. R. Craig, and G.V. Gibbs, Phys. Chem. Minerals, 4 (1979) 317-339.

[34] M. Laarj and S. Kacim, J. Solid State Chem., 125 (1996) 67–74.

[35] R. D. Shannon, Acta Cryst., A, 32 (1976) 751.

[36] G. Srinivasan and Mohindar S. Seehra, Phys. Rev. B, 28 (1983) 28 1.

[37] John E. Greedan, J. Mater. Chem., 11 (2001) 37-53.

[38] O. Peña, Y. Ma, P. Barahona, M. Bahout, P. Duran, C. Moure, M. N. Baibich and G. Martinez, J. Eur. Ceram. Soc., 25 (2005) 3051.

[39] Y. Ma, M. Bahout, O. Peña, P. Duran and C. Moure, Bol. Soc. Esp. Ceram. Vidrio, 43 (2004) 663.

[40] O. Peña, Y. Ma, M. Bahout, P. Duran, C. Moure and M. N. Baibich, Phys. Statussolid (c), 1(S1) (2004) S31.

[41] A. Herpin, Théorie du magnétisme, Presses universitaires de France, Paris, 1968.

[42] J. Van Kranendonk and J. H. Van Vleck, Rev. Mod. Phys., 30 (1958) 1.

[43] J. S. Kouvel and Harvey Brooks, Technical Report No. 198, Gruff Laboratory, Harvard University Cambridge, Massachusetts (1954)

[44]M. L. Glasser and F. J. Milford, Phys. Rev., 130 (1963) 1783.

[45]H. Unruh, Jr. and F. J. Milford, Phys. Rev., 123 (1961) 1619.

[46] F. Bloch, Z. Phys., 74 (1932) 295.

[47]Yu. A. Izyumov and R. P. Ozerov, Magnetic Neutron Diffraction, Plenum Press, New York, 1970.

[48]N. N. Efimova and S. R. Kufterina, Phys. Solid State, 40 (1998) 982.

[49] A. Franco, Jr.V. S. Zapf, V. B. Barbeta and R. F. Jardim, J. Appl. Phys. ,107 (2010) 073904.

[50] T. D. Pierce, R. J. Celotta, J. Unguris, and H. C. Siergmann, Phys. Rev. B, 26 (1982) 2566.

Parameters	Samples				
	1.2	1.3	1.4	1.5	1.6
a(Å)	8.4868(3)	8.4818(2)	8.4775(2)	8.4729(2)	8.4675(2)
O(32e) : u	0.2625(2)	0.2629(2)	0.2634(2)	0.2636(2)	0.2638(2)
Cation distribution Rietveld	$(Mn^{2+}_{0.80(6)}Ga^{3+}_{0.20(6)})_A$ $[Mn^{2+}_{0.20(6)}Mn^{3+}_{0.80(6)}Ga^{3+}]_B$	$(Mn^{2+}_{0.79(1)}Ga^{3+}_{0.21(1)})_A$ $[Mn^{2+}_{0.21(1)}Mn^{3+}_{0.70(1)}Ga^{3+}_{1.09(1)}]_B$	$(Mn^{2+}_{0.76(1)}Ga^{3+}_{0.24(1)})_A$ $[Mn^{2+}_{0.24(1)}Mn^{3+}_{0.60(1)}Ga^{3+}_{1.16(1)}]_B$	$(Mn^{2+}_{0.77(2)}Ga^{3+}_{0.23(2)})_A$ $[Mn^{2+}_{0.23(2)}Mn^{3+}_{0.50(2)}Ga^{3+}_{1.27(2)}]_B$	$(Mn^{2+}_{0.84(2)}Ga^{3+}_{0.16(2)})_A$ $[Mn^{2+}_{0.16(2)}Mn^{3+}_{0.40(2)}Ga^{3+}_{1.44(2)}]_B$
R_P(%)	10.2	8.8	8.6	9.5	9.1
R_{wp} (%)	15.8	13.9	13.5	16.8	14.0
R_{exp} (%)	14.7	13.6	13.3	16.2	13.7
R_{Bragg}(%)	4.4	3.5	3.4	5.3	4.7
R_F (%)	3.9	3.0	3.1	3.6	3.7
χ^2	1.10	1.03	1.02	1.08	1.05
Cation distribution O'Neill Model	$(Mn^{2+}_{0.84}Ga^{3+}_{0.16})_A$ $[Mn^{2+}_{0.16}Mn^{3+}_{0.80}Ga^{3+}_{1.04}]_B$	$(Mn^{2+}_{0.83}Ga^{3+}_{0.17})_A$ $[Mn^{2+}_{0.17}Mn^{3+}_{0.70}Ga^{3+}_{1.13}]_B$	$(Mn^{2+}_{0.82}Ga^{3+}_{0.18})_A$ $[Mn^{2+}_{0.18}Mn^{3+}_{0.60}Ga^{3+}_{1.22}]_B$	$(Mn^{2+}_{0.81}Ga^{3+}_{0.19})_A$ $[Mn^{2+}_{0.19}Mn^{3+}_{0.50}Ga^{3+}_{1.31}]_B$	$(Mn^{2+}_{0.80}Ga^{3+}_{0.20})_A$ $[Mn^{2+}_{0.20}Mn^{3+}_{0.40}Ga^{3+}_{1.40}]_B$
a(Å) Shannon and Rietveld	8.488	8.482	8.477	8.470	8.462
a(Å) Shannon and O'Neill	8.487	8.481	8.475	8.469	8.463

Table 1: Crystal structures (*Fd-3m*), cell parameters (a), oxygen atomic coordinates (u), cation distribution and reliability factors for $Ga_xMn_{(3-x)}O_4$ (x=1.2-1.6) determined from Rietveld refinements using the a4 model. The cation distribution was calculated using O'Neill and Navrotsky's model. Bottom: Theoretical cell parameters calculated using Shannon ionic radii, chemical occupation (determined from Rietveld refinements) and cation distribution (O'Neill Model).

x	C (emu.K/mol)	μ_{eff} (μ_B)	μ_{theo} (μ_B)	$\lvert\mu_{eff} - \mu_{theo}\rvert$ %	T_c (K)	Θ (K)	$f=\theta/T_c$
1.2	6.51(2)	7.22(1)	7.35	1.7%	28(1)	-244	8.7
1.3	6.85(2)	7.40(1)	7.18	3%	24(1)	-238	9.9
1.4	6.77(6)	7.36(3)	7.02	4.8%	19(1)	-212	11.1
1.5	5.94(2)	6.90(1)	6.84	0.8%	16(1)	-197	12.3
1.6	5.47(2)	6.62(1)	6.64	0.3%	14(1)	-189	13.5

Table 2: Results of fits: C Curie-Weiss constant; μ_{eff} experimental magnetic moment, μ_{theo} theoretical magnetic moment, Tc transition temperature, θ Curie-Weiss temperature; f frustration parameter.

x(Ga^{3+})	$M_s(\mu_B$/f.u.) Exp	$M_s(\mu_B$/f.u.) Theo (Néel)	φ_0 (deg)	$\varphi_0+\varphi_1$ (deg)	H_0(T)	B (x10^{-3} $K^{3/2}$)	D (mev.$Å^2$)
1.2	0.61(3)	1.8	19	47	17.6	1.9(1)	53
1.4	0.45(2)	2.6	47	64	10.3	3.5(4)	40
1.5	0.43(2)	3.0	50	71	12.6	1.3(3)	82
1.6	0.32(1)	3.4	53	79	17.7	0.9(1)	135

Table 3: $Ms(\mu_B/f.\ u.)_{exp}$ experimental values of the spontaneous magnetization determined at 2 K, $Ms(\mu_B/f.\ u.)_{theo}$ theoretical values of the spontaneous magnetization calculated using collinear Néel model, φ_0 canting angles at H = ∞, $\varphi_0+\varphi_1$ canting angles at H = 0T, H_0 magnetic interaction parameter, B Bloch's constant, D Spin wave stiffness parameter determined from results of Ms (T) using Bloch's and Dyson equations.

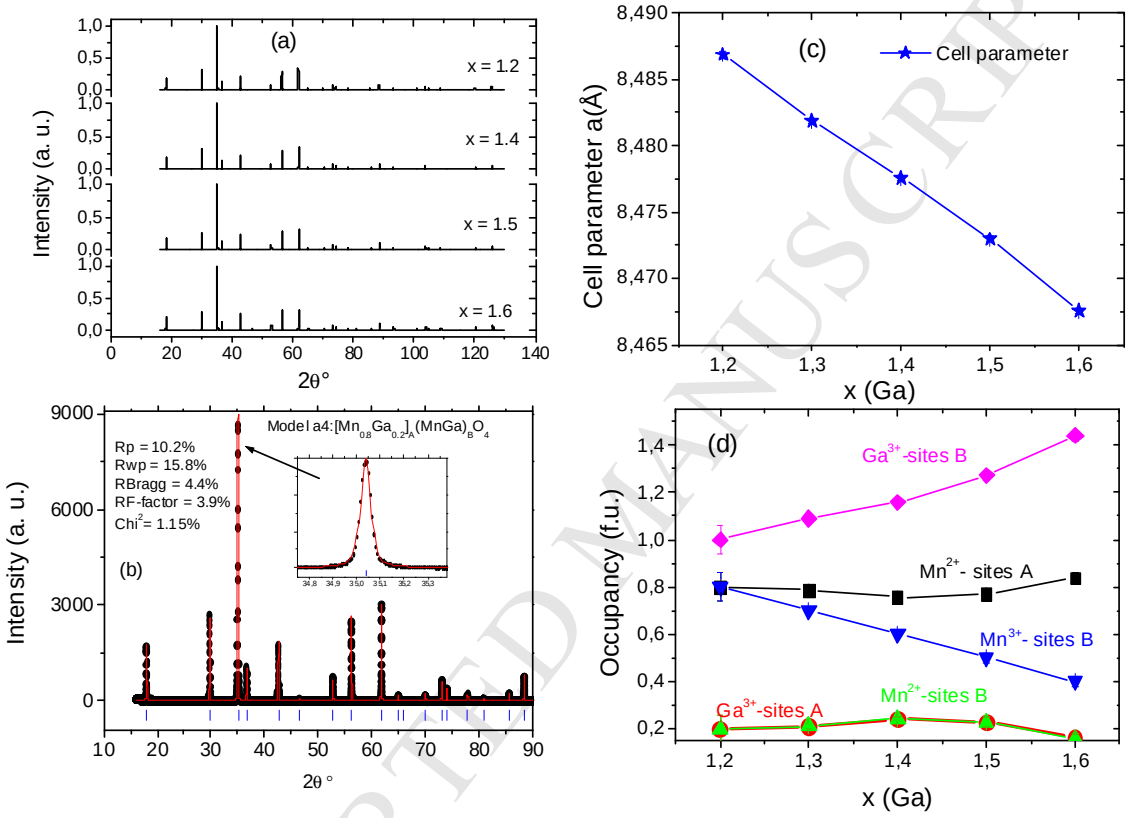

Figure 1: (a) X-ray diffraction patterns for $Ga_xMn_{(3-x)}O_4$(x=1.2-1.6) at room temperature, (b) refined diagram by the Rietveld method using a4 model, (c) evolution of the lattice parameter (a) as function of composition x(Ga^{3+}), (d) occupancy of different cations as a function of x(Ga^{3+}) in tetrahedral and octahedral sites.

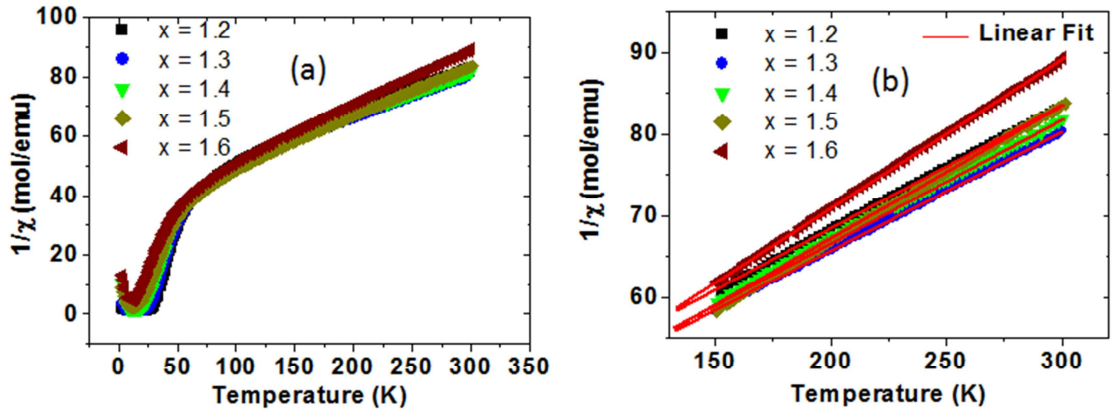

Figure 2: (a) Inverse magnetic susceptibility 1/χ as a function of temperature recorded under a magnetic field of 0.1T for all samples of the $Ga_xMn_{3-x}O_4$ system ($1.2 \leq x \leq 1.6$). (b) 1/χ fit using Curie-Weiss equation in the temperature range from 150 to 300K.

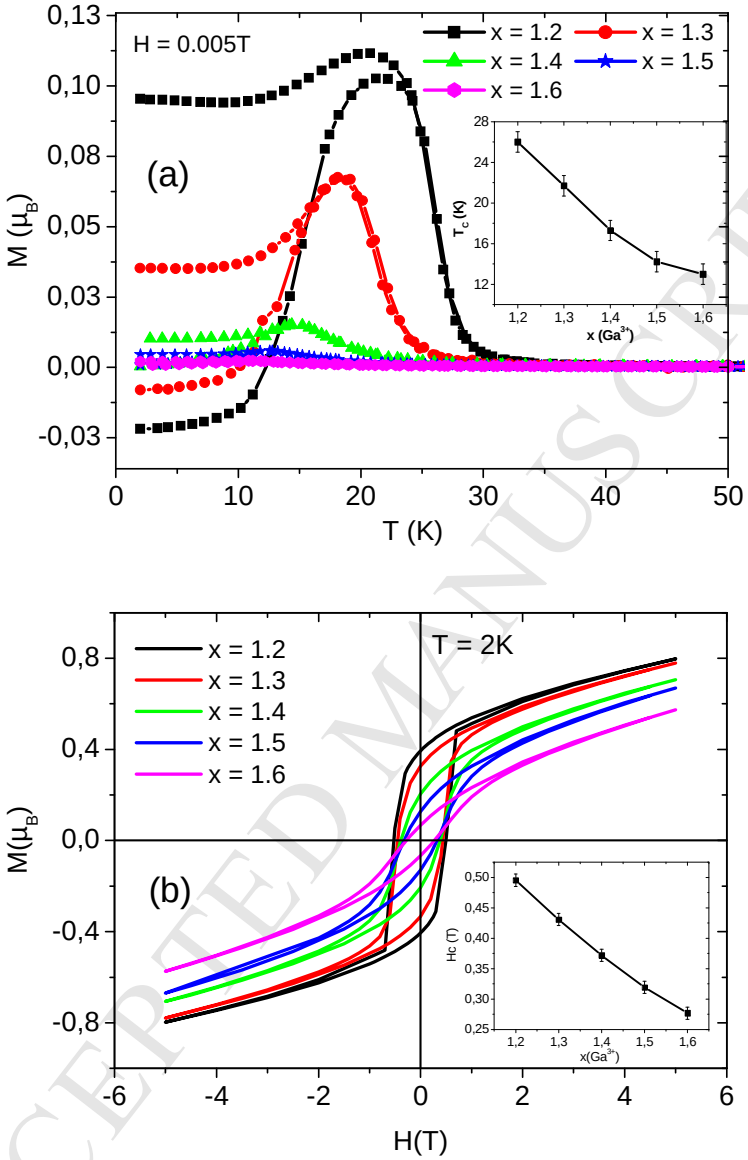

Figure 3: (a) Magnetization as a function of temperature with ZFC/FC modes for different compositions $Ga_xMn_{3-x}O_4$ ($1.2 \leq x \leq 1.6$). Inset (a) The transition temperature T_C vs $x(Ga^{3+})$. (b) Hysteresis loops at 2K. Inset (b) Evolution of the coercive field Hc as a function of $x(Ga^{3+})$.

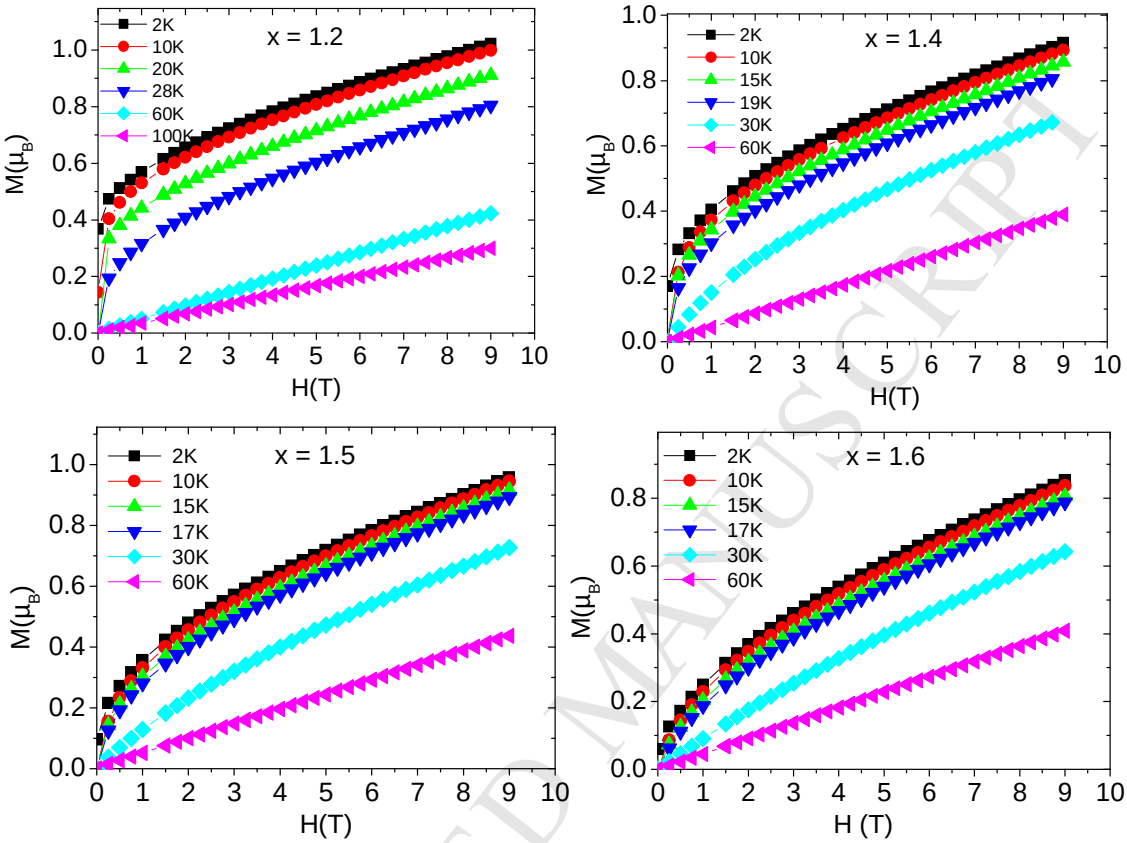

Figure 4: First magnetization curves as a function of magnetic field up to 9T at different temperatures.

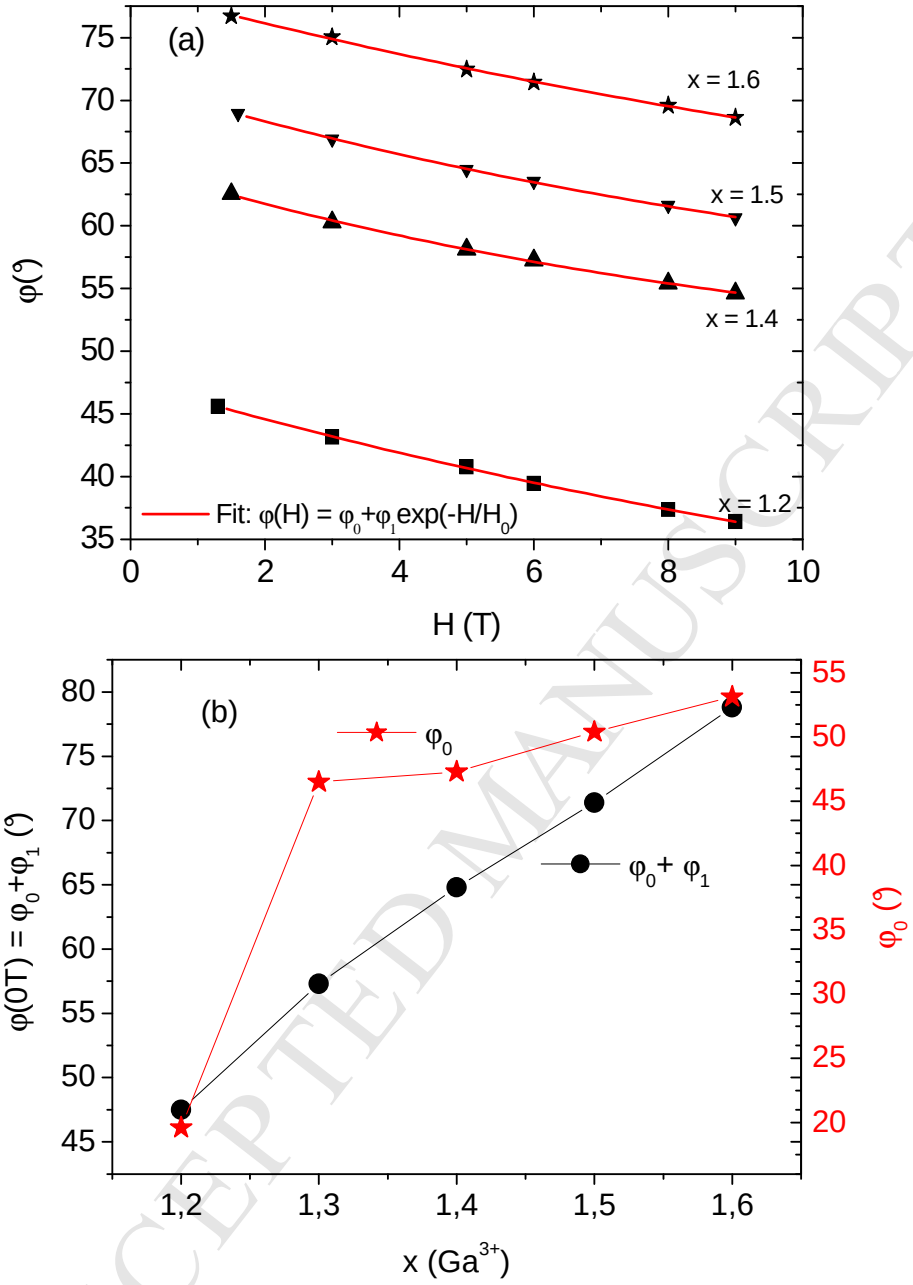

Figure 5: (a) Evolution of the angle φ(H) as a function of the magnetic field, together with the fit of φ(H) curves obtained using the equation: $\varphi(H) = \varphi_0 + \varphi_1 e^{\frac{-H}{H_0}}$. (b) angle φ_0 of the magnetic structure at strong magnetic field (H→∞), and the $\varphi_0 + \varphi_1$ angle of the magnetic structure at H=0T of each compound.

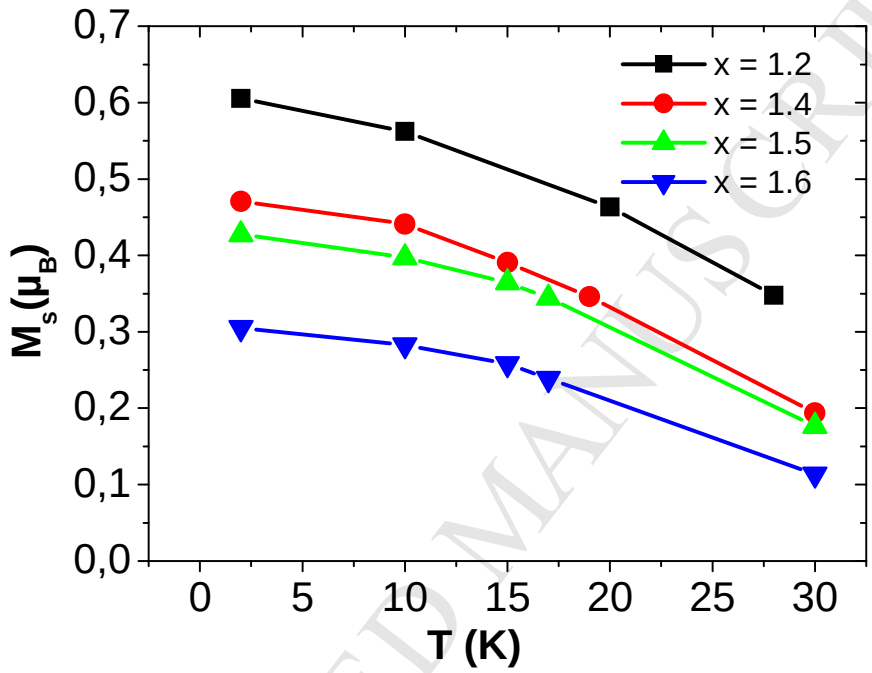

Figure 6: Temperature dependence of spontaneous magnetization Ms (T) determined by extrapolation of the linear part of M(H) (fig. 4) to H = 0T.

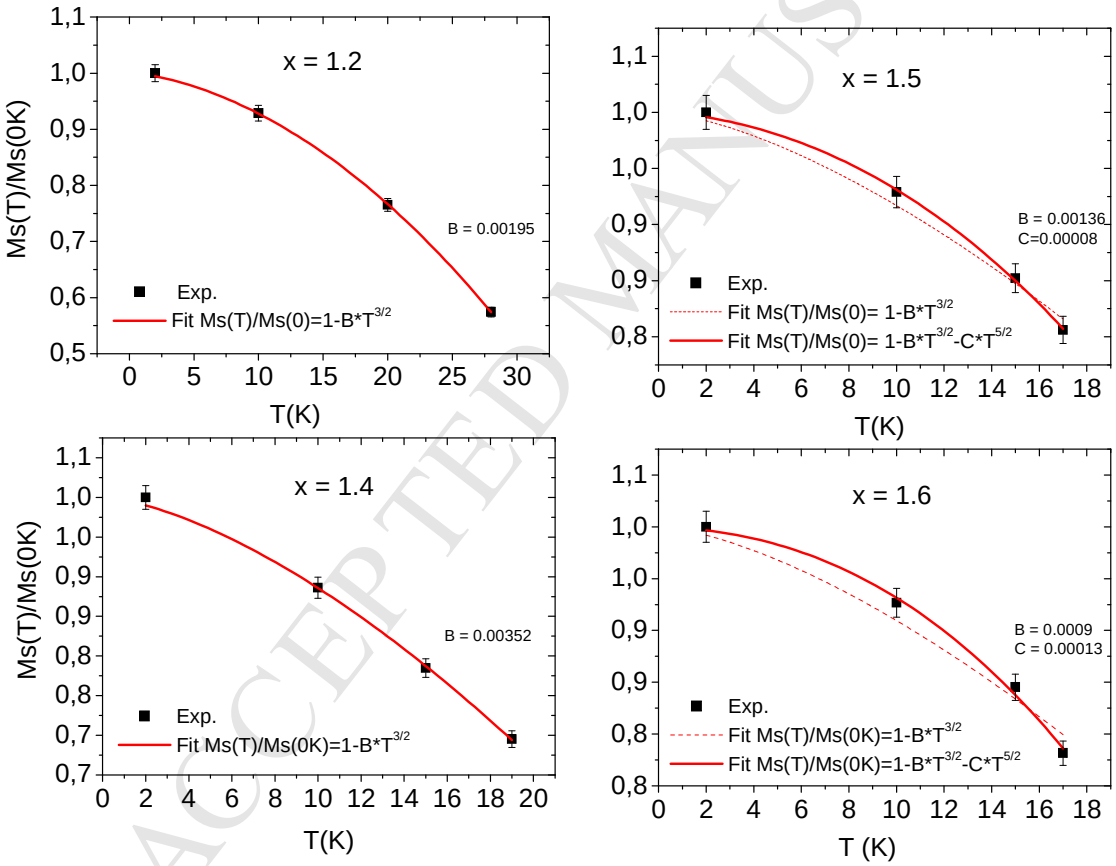

Figure 7: Fitting results of Ms(T) curves using equations (8) and (10).

Highlights

- $Ga_xMn_{(3-x)}O_4$ ($1.2 \leq x \leq 1.6$) compounds prepared by solid-state reaction.
- Cation distribution and crystallographic parameters have been determined using Rietveld method and O'Neill and Navrotsky model.
- Spin wave stiffness parameters were determined for each composition
- Compounds x = 1.2-1.4 present a non-collinear ferrimagnetic order.
- Compounds x = 1.5-1.6 present a frustrated non-collinear ferrimagnetic order.